

# Permanent Magnet Hybrid Core Inductors for High Saturation Capability

RACHEL S. YANG<sup>1</sup> (Student Member, IEEE), ANDREW B. NADLER<sup>2</sup> (Graduate Student Member, IEEE),  
CHARLES R. SULLIVAN<sup>1</sup> (Fellow, IEEE), AND DAVID J. PERREAU<sup>1</sup> (Fellow, IEEE)

<sup>1</sup>Massachusetts Institute of Technology, Cambridge, MA 02139 USA  
<sup>2</sup>Thayer School of Engineering, Dartmouth College, Hanover, NH 03775 USA

CORRESPONDING AUTHOR: RACHEL S. YANG (e-mail: rsyang@mit.edu)

*This paper was presented in part at the 2022 IEEE Workshop on Control and Modeling for Power Electronics (COMPEL) and extends that work by providing additional theoretical analysis, example implementations, simulations, and experimental results. [DOI: 10.1109/COMPEL53829.2022.9830021].*

This work was supported in part by pSemi, in part by the National Science Foundation Graduate Research Fellowship under Grants 1745302 and 2141064, and in part by the E.E. Landsman (1958) Fellowship.

**ABSTRACT** Inductor designs with large dc current relative to ac ripple are often constrained by saturation, which limits their size, loss, and current-carrying capability. Typical saturation-limited designs, though, further handicap their performance by substantially underutilizing their core material's flux carrying capabilities. Instead of operating the core across its full flux swing range from reverse saturation to forward saturation, these designs only use half the range. To use the full range, we propose a permanent magnet (PM) hybrid core in which a PM provides a dc flux offset in the core, boosting its effective saturation capability. In the proposed core, the PM is placed outside of the main winding flux path to reduce losses and risk for PM demagnetization. In this work, we derive first-order theory for analyzing and designing the PM hybrid core. We then provide some example PM hybrid core implementations. Finally, we demonstrate a working proof-of-concept prototype using off-the-shelf parts that outperforms two comparable ferrite inductor designs. This PM hybrid core prototype achieves half the dc resistance of a ferrite inductor with the same energy storage, and it achieves 70% more energy storage than a ferrite inductor with the same dc resistance. The prototype's improved performance thus demonstrates the potential advantages of the PM hybrid core.

**INDEX TERMS** Inductors, magnetics, permanent magnets, saturation flux density.

## I. INTRODUCTION

Many power electronics applications require inductors having small ac current ripple relative to their dc current (i.e. small ripple ratio), such as in filters and converters in continuous conduction mode. In these applications, inductors are often the limiting component in terms of size, loss, or current-carrying capability. The design of these small-ripple-ratio inductors is usually limited by saturation constraints, where for a given flux density limit, the designer is forced to trade off achievable energy storage density with loss (via number of turns). Core materials with high saturation flux densities can improve the achievable energy storage density. But, as power electronics shift to higher frequency operation, these materials also need good high-frequency core loss characteristics for the ac ripple current, especially since core loss can increase

with dc bias [2], [3]. Ferrites are a good candidate material as they generally have low core loss at high frequencies [4], [5], but they also usually have low saturation flux densities ( $B_{sat} < 0.5$  T) [6], [7], limiting dc performance.

Furthermore, inductor designs for saturation-limited cases usually underutilize the saturation flux density range of the core material. To visualize this, we examine the saturation behavior of a core material using a BH curve, neglecting hysteresis effects (Fig. 1). In dc-dominated applications, the current, and thus  $H$  fields, are non-negative, which means the core only operates on the positive side of the BH curve. So, while the core can handle flux densities from  $-B_{sat}$  to  $B_{sat}$ , the inductor only uses half of this range from 0 to  $B_{sat}$ , greatly underutilizing the core's potential. But, if the BH curve could be offset to the right, the core could use more of its

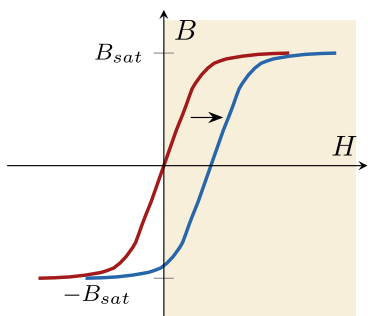


**FIGURE 1.** Shifting the BH curve to the right enables a core to use more of its saturation flux density range in dc-dominated applications.

saturation range. In particular, if the curve is offset so that reverse saturation starts at  $H = 0$ , or zero current, the core could use its full saturation range. In this case, materials such as ferrites may still achieve good saturation performance, despite having a low  $B_{sat}$ .

One possibility for offsetting the BH curve is to use a permanent magnet (PM) to oppose dc winding flux in the ferrite or other soft magnetic material. The resulting core operates for a wider range of unipolar winding flux. Previously, PMs have been used in inductors to improve saturation performance [8], [9], [10], [11], [12], [13], [14], [15], [16], [17]. These inductors, however, often position the PMs in or next to gaps, which puts them fully or at least partly in the winding flux path. Due to this placement, the PM is at risk for demagnetization at large currents [9], [18] and can incur ac loss, which increases with frequency [19]. For lower ac loss, ferrite permanent magnets may be used, but their low remanent flux limits the benefit they can offer.

One previous PM inductor design [20] has proposed reducing demagnetization risk and ac loss in the PM by placing it outside the winding flux path. To do so, this design intentionally saturates part of the core's soft magnetic material.

This work proposes alternative PM hybrid core designs in which a PM opposes the dc winding flux in a soft magnetic core material without intentionally saturating part of the core. Unlike most previous work, these designs avoid subjecting the PM to significant winding flux. By doing so, they can achieve large flux carrying capabilities without incurring ac loss in the PM, thus making them suitable for applications that have large dc flux with high-frequency flux ripple.

In this article, we focus on PM hybrid cores that combine PMs with ferrites. The developed theory, however, is general and can apply to other soft magnetic materials, such as powdered iron cores. In Section II, we derive first-order models for designing the PM hybrid core and compare its performance with that of a pure ferrite core. In Section III, we discuss possible implementations of the PM hybrid core. Finally, in Section IV, we show a working proof-of-concept PM hybrid inductor using off-the-shelf parts. This inductor outperforms two comparable ferrite inductors in both simulation and experiment. For a fixed energy storage, the PM hybrid prototype achieves half the dc resistance of a ferrite inductor. For a fixed

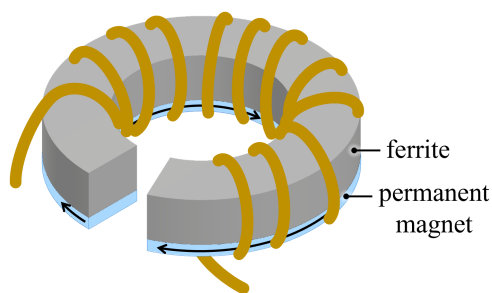


**FIGURE 2.** Simple example implementation of the PM hybrid core. The PM and ferrite are in parallel with each other, with the ferrite using some fraction  $F_f$  of the total core area. The PM is magnetized in the azimuthal  $\phi$  direction, and the entire core cross-section is gapped.

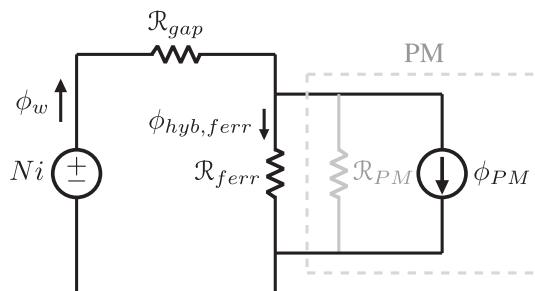


**FIGURE 3.** Simple idealized magnetic circuit model for the PM hybrid core. Often,  $\mathcal{R}_{PM} \gg \mathcal{R}_{ferr}$  so  $\mathcal{R}_{PM}$  can be ignored.

dc resistance, the PM hybrid prototype achieves 70% more energy storage than a ferrite inductor.

## II. THEORY FOR PERMANENT MAGNET HYBRID CORES

In this section, we develop first-order theory for the proposed PM hybrid core's operation and performance. To do this, we look at a simple example implementation of the core using a toroid geometry, where the PM is placed in parallel with the ferrite core and is magnetized in the azimuthal  $\phi$  direction (Fig. 2). Here, the entire hybrid core cross-section is gapped, and the PM and ferrite have the same core lengths. For a fixed core area  $A_c$ , the ferrite uses some fraction  $F_f$  of the area, while the PM uses the rest  $(1 - F_f)$ .

We can model the PM hybrid core using a simple idealized magnetic circuit, shown in Fig. 3. In this model, we neglect the effects of lateral flux transfer between the PM and ferrite. We use a Norton model for the PM, with a flux source  $\phi_{PM}$  set by the PM's remanent flux density  $B_r$  and cross-sectional area  $A_{PM}$  using  $\phi_{PM} = B_r A_{PM} = B_r A_c (1 - F_f)$ . The PM's reluctance  $\mathcal{R}_{PM}$  can be roughly modeled using its length  $l_{PM}$  and permeability  $\mu_{PM}$  as  $\mathcal{R}_{PM} \approx \frac{l_{PM}}{\mu_{PM} A_{PM}}$ , with  $\mu_{PM}$  usually being very close to  $\mu_0$ . The maximum flux that the ferrite part of the core can carry is set by the ferrite's maximum allowed flux density<sup>1</sup>  $B_{max}$  and cross-sectional area  $A_{ferr}$  using  $\phi_{max,hyb,ferr} = B_{max} A_{ferr} = B_{max} A_c F_f$ .

<sup>1</sup>The maximum allowed flux density  $B_{max}$  can be the saturation flux density  $B_{sat}$  of the ferrite or some fraction of  $B_{sat}$ . For example,  $B_{max}$  can be chosen below  $B_{sat}$  at a point before the material's incremental permeability drops off.

### A. IDEAL PM HYBRID CORE CHARACTERISTICS

To develop intuition for the PM hybrid core's design and characteristics, we first consider its operation using a set of idealized approximations. Considering the reluctances  $\mathcal{R}$  of the magnetic circuit, we assume that the ferrite has a permeability sufficiently larger than  $\mu_{PM} \approx \mu_0$  for  $\mathcal{R}_{ferr} \ll \mathcal{R}_{PM}$  and that the gap dominates the winding flux path for  $\mathcal{R}_{ferr} \ll \mathcal{R}_{gap}$ . So, in Fig. 3, the winding flux  $\phi_w$  from the mmf source  $Ni$  primarily flows through the gap and the ferrite, and the PM flux  $\phi_{PM}$  flows primarily through the ferrite in the opposite direction. The PM thus offsets the flux in the ferrite without being in the main path of the winding flux and incurring ac losses.

Using the model of Fig. 3 and the above idealized assumptions, we derive first-order models for optimizing the PM hybrid core as well as its optimized characteristics. First, we model the PM hybrid core's maximum flux carrying capability  $\phi_{\max,hyb}$ , which is determined by the ferrite part's maximum allowed flux  $\phi_{\max,hyb,ferr}$  and the flux offset provided by the PM  $\phi_{PM}$ . We can mathematically represent  $\phi_{\max,hyb}$  as

$$\begin{aligned}\phi_{\max,hyb} &= \phi_{\max,hyb,ferr} + \phi_{PM} \\ &= B_{\max}A_cF_f + B_rA_c(1 - F_f) \\ &= B_rA_c + F_f(B_{\max} - B_r)A_c\end{aligned}\quad (1)$$

Per (1), for a given set of materials and a fixed core area  $A_c$ , we can control  $\phi_{\max,hyb}$  via the fraction of ferrite  $F_f$  used. As we decrease  $F_f$  and devote more area to the PM, more PM flux is available to oppose the winding flux in the ferrite, thus increasing the hybrid core's flux carrying capability.

To help understand which materials would be most useful in a PM hybrid core, let's examine (1) in more detail. For a given set of materials, (1) is a linear function of  $F_f$  having a slope of  $(B_{\max} - B_r)$ . Here, a negative slope implies that reducing the fraction of ferrite  $F_f$  and adding more PM improves  $\phi_{\max,hyb}$ , while a positive slope implies that the addition of PM hurts performance. So, for the PM hybrid core to be advantageous with a negative slope,  $B_r$  of the PM must be greater than  $B_{\max}$  of the ferrite ( $B_r > B_{\max}$ ). Otherwise, the PM hybrid would be trading a fraction of ferrite for a PM material with worse flux characteristics.

To maximize  $\phi_{\max,hyb}$  in (1) with  $B_r > B_{\max}$ , we want  $F_f$  to be as small as possible. But (1) only considers the PM hybrid core's saturation behavior at large currents and not at small currents, where the PM flux may reverse saturate the ferrite. To prevent reverse saturation at zero current and above, we must ensure that the PM flux does not exceed the ferrite's maximum flux capability, i.e.  $\phi_{PM} \leq \phi_{\max,hyb,ferr}$ . But to maximize the PM hybrid core's flux carrying capability, we want the PM flux to be as large as possible and thus set  $\phi_{PM} = \phi_{\max,hyb,ferr} = B_{\max}A_cF_f$ . By substituting this reverse saturation constraint into the first line of (1), we get that the maximum PM hybrid core flux is  $2B_{\max}A_cF_f$ , or twice the flux carrying capability of the ferrite area. In this case, the PM is exactly offsetting the ferrite's BH curve so that we're using its full range from  $-B_{\max}$  to  $B_{\max}$ .

Next, we can solve for the fraction of ferrite  $F_f$  that gives us this optimal flux carrying capability. From the PM's geometry, we know that  $\phi_{PM} = B_rA_c(1 - F_f)$ . By combining this with the reverse saturation constraint  $\phi_{PM} = B_{\max}A_cF_f$ , we get that the optimal ferrite fraction is

$$F_{f,opt} = \frac{B_r}{B_r + B_{\max}}\quad (2)$$

We can also solve for the PM hybrid core's maximum flux carrying capability by substituting (2) into (1):

$$\phi_{\max,hyb} = \frac{2B_rB_{\max}}{B_r + B_{\max}}A_c = 2\frac{B_{\max}}{1 + \frac{B_{\max}}{B_r}}A_c\quad (3)$$

Based on this result, we can find an effective maximum flux density  $B_{\max,eff}$  for a uniform core providing the same flux-carrying capability such that  $\phi_{\max,hyb} = B_{\max,eff}A_c$ :

$$B_{\max,eff} = \frac{2B_rB_{\max}}{B_r + B_{\max}} = 2\frac{B_{\max}}{1 + \frac{B_{\max}}{B_r}}\quad (4)$$

The intermediate form of  $B_{\max,eff}$  can also be rewritten as  $B_{\max,eff} = 2(B_r || B_{\max})$ , suggesting that the PM hybrid core acts equivalently as two parallel materials (PM and ferrite) using their full saturation flux density range.

To better understand the benefits of the PM hybrid core, we compare its performance with that of a pure ferrite core having the same volume and core area. For a ferrite core, its maximum achievable flux is  $\phi_{\max,ferr} = B_{\max}A_c$ . From (3) and (4), we see that the PM hybrid core achieves a larger maximum flux and effective flux density than the pure ferrite core by a factor of  $\frac{2}{1 + \frac{B_{\max}}{B_r}}$ . This improvement can be substantial. For example, suppose we use a NdFeB PM of grade N40SH with  $B_r = 1.285$  T and Ferroxcube 3F46 ferrite with  $B_{sat} = 0.43$  T at 100 °C. We set  $B_{\max} = 0.75B_{sat} = 0.32$  T to remain in the linear region of the BH curve. In this example, the PM hybrid core can achieve 1.6x greater effective maximum flux (and flux density) than a pure ferrite core. Such a PM hybrid core design would have an optimal ferrite fraction of  $F_{f,opt} = 0.80$ , per (2), with a PM using the rest of the core area.

To provide intuition for these results, we examine what happens as  $B_r \rightarrow \infty$ . In this limit,  $F_{f,opt} \rightarrow 1$  because we only need a tiny fraction of PM in the core to enable the ferrite to use its full saturation flux density range without reverse saturating at zero current. Then, because very little ferrite area is removed, the PM hybrid core can achieve double the flux range of a pure ferrite core, with  $\phi_{\max,hyb} \rightarrow 2B_{\max}A_c$ .

### B. REFINED PM HYBRID CORE CHARACTERISTICS

In the previous subsection, we assumed  $\mathcal{R}_{ferr} \ll \mathcal{R}_{gap}$  so that approximately all of the PM flux returns through the ferrite. It's possible, though, to have a design where  $\mathcal{R}_{ferr} \ll \mathcal{R}_{gap}$ . For example, the core could have a relatively small gap, or the chosen ferrite could have relatively low permeability. In this case, a non-negligible amount of the PM flux may cross the gap instead.

To include this effect in our models, we model the PM hybrid core with an *effective* PM return flux, where only

**TABLE 1. Optimal Ferrite Fraction  $F_{f,opt}$  and Maximum Flux Carrying Capability  $\phi_{max}$  for the Pure Ferrite and PM Hybrid Cores. In the Refined PM Hybrid Core Model,  $k_{PM}$  is the Calculated Fraction of PM Flux That Returns Through the Ferrite Part of the Core**

	Pure Ferrite	PM Hybrid (Ideal)	PM Hybrid (Refined)
$F_{f,opt}$	1	$\frac{B_r}{B_r + B_{max}}$	$\frac{B_r}{B_r + \frac{B_{max}}{k_{PM}}}$
$\phi_{max}$	$B_{max}A_c$	$2\frac{B_{max}}{1 + \frac{B_{max}}{B_r}}A_c$ or $2(B_{max}  B_r)A_c$	$2\frac{B_{max}}{1 + \frac{B_{max}}{k_{PM}B_r}}A_c$ or $2(B_{max}  k_{PM}B_r)A_c$

a fraction  $k_{PM}$  of the PM flux returns through the ferrite ( $\phi_{PM,eff} = k_{PM}\phi_{PM}$ ). With this refinement, the hybrid core's maximum flux carrying capability becomes

$$\begin{aligned}\phi_{max,hyb} &= \phi_{max,hyb,ferr} + \phi_{PM,eff} \\ &= B_{max}A_cF_f + k_{PM}B_rA_c(1 - F_f) \\ &= k_{PM}B_rA_c + F_f(B_{max} - k_{PM}B_r)A_c\end{aligned}\quad (5)$$

Based on (5) and using analogous arguments from the previous subsection, we can conclude that the PM hybrid core is only advantageous when the effective  $B_r$  of the PM is greater than  $B_{max}$  of the ferrite ( $k_{PM}B_r > B_{max}$ ). So, for a given set of materials, a minimum  $k_{PM} = B_{max}/B_r$  is needed for the PM to do useful work.

Refined expressions for key characteristics of the PM hybrid core, which incorporate effective PM flux, are listed in Table 1. In the refined model, less PM flux effectively offsets the flux in the ferrite compared to the ideal model, so more PM area is needed in a refined optimized design, for  $F_{f,opt,ref} < F_{f,opt,ideal}$ . With less ferrite area, the refined core model also carries less total flux than the ideal model, so  $\phi_{max,hyb,ref} < \phi_{max,hyb,ideal}$ .

For some intuition for the impact of  $k_{PM}$  on the PM hybrid core, we can examine the results of Table 1 in its limits. As we approach the minimum useful value of  $k_{PM}$  ( $k_{PM} \rightarrow B_{max}/B_r$ ), the effective flux carrying capability of the PM hybrid core design approaches that of a pure ferrite core ( $\phi_{max,hyb} \rightarrow \phi_{max,ferr}$ ), as the PM's effective flux characteristics approach the ferrite's. In this lower limit, the PM hybrid core also approaches a lower bound on  $F_{f,opt,rev} \rightarrow 0.5$ , dividing the area evenly between the two similarly-behaving materials. As  $k_{PM} \rightarrow 1$ , the refined model approaches the ideal characteristics derived in the previous subsection.

There are many possible models for  $k_{PM}$ , depending on how the PM hybrid core is modeled. One  $k_{PM}$  model can be derived from the magnetic circuit in Fig. 3. Again, we treat the PM reluctance  $\mathcal{R}_{PM}$  as relatively large and approximate it as an open circuit. We can then analyze the PM flux return path as a flux divider between the ferrite ( $\mathcal{R}_{ferr}$ ) and gap ( $\mathcal{R}_{gap}$ ). In this case, the amount of PM flux that returns through the ferrite is

$$\phi_{PM,eff} = \frac{\mathcal{R}_{gap}}{\mathcal{R}_{gap} + \mathcal{R}_{ferr}}\phi_{PM}, \text{ which gives us}$$

$$k_{PM} = \frac{\mathcal{R}_{gap}}{\mathcal{R}_{gap} + \mathcal{R}_{ferr}} = \frac{1}{1 + \frac{\mathcal{R}_{ferr}}{\mathcal{R}_{gap}}}\quad (6)$$

This model behaves as expected in the limit of large and small gaps. As  $\mathcal{R}_{gap} \rightarrow \infty$ ,  $k_{PM} \rightarrow 1$ , approaching the ideal model. As  $\mathcal{R}_{gap} \rightarrow 0$ ,  $k_{PM} \rightarrow 0$  for zero PM return flux.

To better understand how strongly  $k_{PM}$  affects PM hybrid core designs, we consider designs using the example set of materials from the end of Section II-A. The PM (N40SH) has  $B_r = 1.285$  T, and the ferrite (3F46) has  $B_{sat} = 0.43$  T at 100 °C and relative permeability  $\mu_r = 750$ . Again, we set  $B_{max} = 0.75B_{sat}$  to remain in the BH curve's linear region.

Fig. 4 compares the ideal and refined PM hybrid core characteristics for this example across ratios of gap and ferrite reluctances ( $\mathcal{R}_{gap}/\mathcal{R}_{ferr}$ ). In this figure, the maximum flux carrying capability  $\phi_{max}$  of the PM hybrid core is normalized to that of a pure ferrite core. As expected, as the reluctance ratio increases for a larger  $k_{PM}$  (such as in designs with relatively large gaps), the refined PM hybrid characteristics

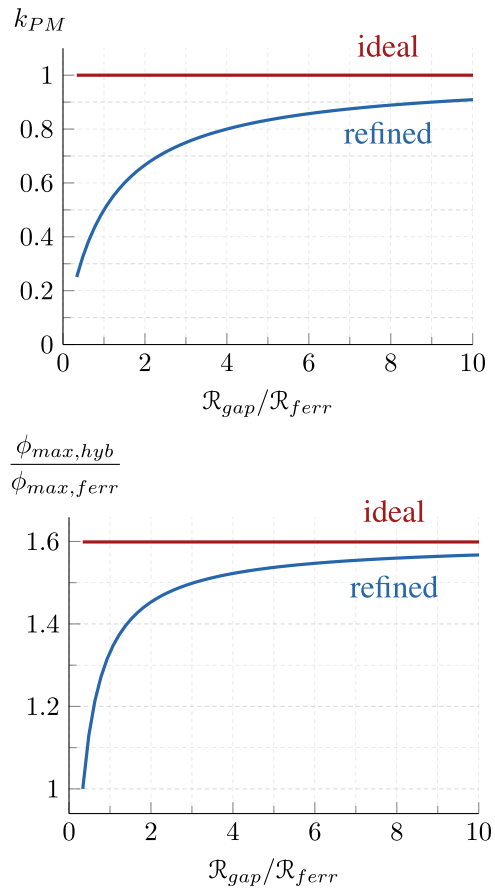


**FIGURE 4. Key characteristics of the PM hybrid core using the ideal and refined models. As the ratio of gap to ferrite reluctance increases, the refined model approaches the ideal model. (Top) Effective PM return flux factor  $k_{PM}$  using the model from (6). (Bottom) Maximum flux carrying capability of the PM hybrid core, normalized to that of a pure ferrite core.**

**TABLE 2. Summary of Additional Performance Metrics Comparing the Ideal PM Hybrid Core Model With a Pure Ferrite Core. Example Comparisons Using a N40SH PM ( $B_r = 1.285$  T) and 3F46 Ferrite ( $B_{\max} = 0.75B_{\text{sat}} = 0.32$  T at  $100^\circ\text{C}$ ) are Also Included**

Metric	Factor of Improvement	Example
max energy storage (fixed $R_{dc}$ and $L$ )	$\frac{ES_{hyb}}{ES_{ferr}} = \left( \frac{2}{1 + \frac{B_{\max}}{B_r}} \right)^2$	2.56x
min $R_{dc}$ (fixed ES and $L$ )	$\frac{R_{dc,hyb}}{R_{dc,ferr}} = \left( \frac{1 + \frac{B_{\max}}{B_r}}{2} \right)^2$	0.39x
max energy storage (fixed dc loss)	$\frac{ES_{hyb}}{ES_{ferr}} = \frac{2}{1 + \frac{B_{\max}}{B_r}}$	1.6x

approach the ideal model. As the ratio decreases, the refined PM hybrid flux capability approaches that of a pure ferrite core, with  $k_{PM} \rightarrow B_{\max}/B_r \approx 0.25$ , as expected.

Fig. 4 also provides insight into which PM hybrid designs can perform near the ideal characteristics. For PM hybrid designs to achieve  $\phi_{\max}$  within 95% of the ideal, we need  $\mathcal{R}_{gap}/\mathcal{R}_{ferr} > 3.9$ , which corresponds to  $k_{PM} > 0.80$ . For a pot core of size P22/13/I with an effective core length  $l_{ferr} = 33.3$  mm, for example, we would need a minimum gap length of  $l_{gap} > 0.17$  mm to achieve this performance. For  $\phi_{\max}$  within 90% of the ideal, we need  $\mathcal{R}_{gap}/\mathcal{R}_{ferr} > 1.8$ , which corresponds to  $k_{PM} > 0.64$  and in a P22/13/I pot core,  $l_{gap} > 0.08$  mm. So, even modest values of  $k_{PM}$  can still yield near-ideal PM hybrid designs.

### C. ADDITIONAL PERFORMANCE ADVANTAGES

In Sections II-A and II-B, we showed that the PM hybrid core can achieve greater maximum flux carrying capability  $\phi_{\max}$  than a pure ferrite core. This improvement can translate into various performance advantages, depending on how the greater  $\phi_{\max}$  is leveraged. Here, we examine three possible metrics for comparing the PM hybrid and ferrite cores, each having the same volume and core area:

- 1) maximum energy storage for a fixed dc resistance ( $R_{dc}$ ) and inductance ( $L$ )
- 2) minimum  $R_{dc}$  for a fixed energy storage and  $L$
- 3) maximum energy storage for a fixed dc loss

For these comparisons, we use the ideal model for the PM hybrid core. For each metric, we calculate the PM hybrid core's improvement over the ferrite core. We then evaluate an example comparison using the example materials from the end of Section II-A, with a N40SH PM ( $B_r = 1.285$  T) and 3F46 ferrite ( $B_{\text{sat}} = 0.43$  T at  $100^\circ\text{C}$ ). Again, we set  $B_{\max} = 0.75B_{\text{sat}} = 0.32$  T to remain in the linear region of the BH curve. A summary of the comparison results and examples are listed in Table 2.

First, we compare the maximum energy storage of the PM hybrid and ferrite cores for a fixed  $R_{dc}$  and inductance  $L$ . Since  $R_{dc}$  is fixed, the number of turns  $N$  is also fixed. In this case, the energy storage for each inductor is determined by its

saturation current, which depends on its maximum achievable flux:  $I_{\text{sat}} = N\phi_{\max}/L$ . The PM hybrid core thus has greater energy storage compared to the ferrite core by a factor of

$$\frac{ES_{hyb}}{ES_{ferr}} = \frac{\frac{1}{2}LI_{\text{sat,hyb}}^2}{\frac{1}{2}LI_{\text{sat,ferr}}^2} = \frac{\phi_{\max,hyb}^2}{\phi_{\max,ferr}^2} = \left( \frac{2}{1 + B_{\max}/B_r} \right)^2 \quad (7)$$

Using the example values  $B_r = 1.285$  T and  $B_{\max} = 0.32$  T, the PM hybrid core can achieve a factor of 2.56x in energy storage than the ferrite core at a fixed  $R_{dc}$  and inductance.

Second, we compare the minimum  $R_{dc}$  of the two cores at a fixed energy storage and inductance. We assume the cores have the same winding area  $A_w$ , winding fill factor  $K_u$ , and mean length of turn  $l_{\text{turn}}$ . For each core, the total dc resistance is  $R_{dc} = NR_{dc,\text{turn}} = N(\rho_{cu} \frac{l_{\text{turn}}}{A_w K_u})/N = N^2 \frac{\rho_{cu} l_{\text{turn}}}{A_w K_u}$ . The number of turns in each core also depends on the maximum achievable flux:  $N = LI_{\text{sat}}/\phi_{\max}$ . Thus, the PM hybrid core can reduce  $R_{dc}$  compared to the ferrite core by a factor of

$$\frac{R_{dc,hyb}}{R_{dc,ferr}} = \frac{N_{hyb}^2 \frac{\rho_{cu} l_{\text{turn}}}{A_w K_u}}{N_{ferr}^2 \frac{\rho_{cu} l_{\text{turn}}}{A_w K_u}} = \frac{\phi_{\max,ferr}^2}{\phi_{\max,hyb}^2} = \left( \frac{1 + B_{\max}/B_r}{2} \right)^2 \quad (8)$$

For example values  $B_r = 1.285$  T and  $B_{\max} = 0.32$  T, the PM hybrid core can achieve an  $R_{dc}$  that is a factor of 0.39x that of the ferrite core at a fixed energy storage and inductance.

Finally, we compare the maximum energy storage of the two cores at a fixed dc loss  $P_{dc,\text{max}}$ . For dc-dominated applications, dc loss is roughly equal to the total loss, and thus, a fixed dc loss approximates a fixed temperature rise. At maximum energy storage, the design's dc loss is  $P_{dc,\text{max}} = I_{\text{sat}}^2 R_{dc} = I_{\text{sat}}^2 N^2 \frac{\rho_{cu} l_{\text{turn}}}{A_w K_u}$ . To maximize energy storage at this loss, each core must operate at its maximum flux density  $B_{\max}$  by satisfying  $LI_{\text{sat}} = N\phi_{\max}$  [21]. Combining these two equations to eliminate  $N$ , the maximum energy storage at  $P_{dc,\text{max}}$  is  $\frac{1}{2}LI_{\text{sat}}^2 = \frac{1}{2}\phi_{\max} \sqrt{\frac{P_{dc,\text{max}} A_w K_u}{\rho_{cu} l_{\text{turn}}}}$ . Assuming both inductors have the same winding geometries, the PM hybrid core has a greater maximum energy storage compared to the ferrite core by a factor of

$$\frac{ES_{\max,hyb}}{ES_{\max,ferr}} = \frac{\frac{1}{2}\phi_{\max,hyb} \sqrt{\frac{P_{dc,\text{max}} A_w K_u}{\rho_{cu} l_{\text{turn}}}}}{\frac{1}{2}\phi_{\max,ferr} \sqrt{\frac{P_{dc,\text{max}} A_w K_u}{\rho_{cu} l_{\text{turn}}}}} = \frac{\phi_{\max,hyb}}{\phi_{\max,ferr}} = \frac{2}{1 + B_{\max}/B_r} \quad (9)$$

For example values  $B_r = 1.285$  T and  $B_{\max} = 0.32$  T, the PM hybrid core can achieve a factor of 1.6x the maximum energy storage of the ferrite core at a fixed dc loss (and roughly, at a fixed total loss or temperature rise).

For the three performance metrics discussed above, the PM hybrid core's improvement over the ferrite core increases as

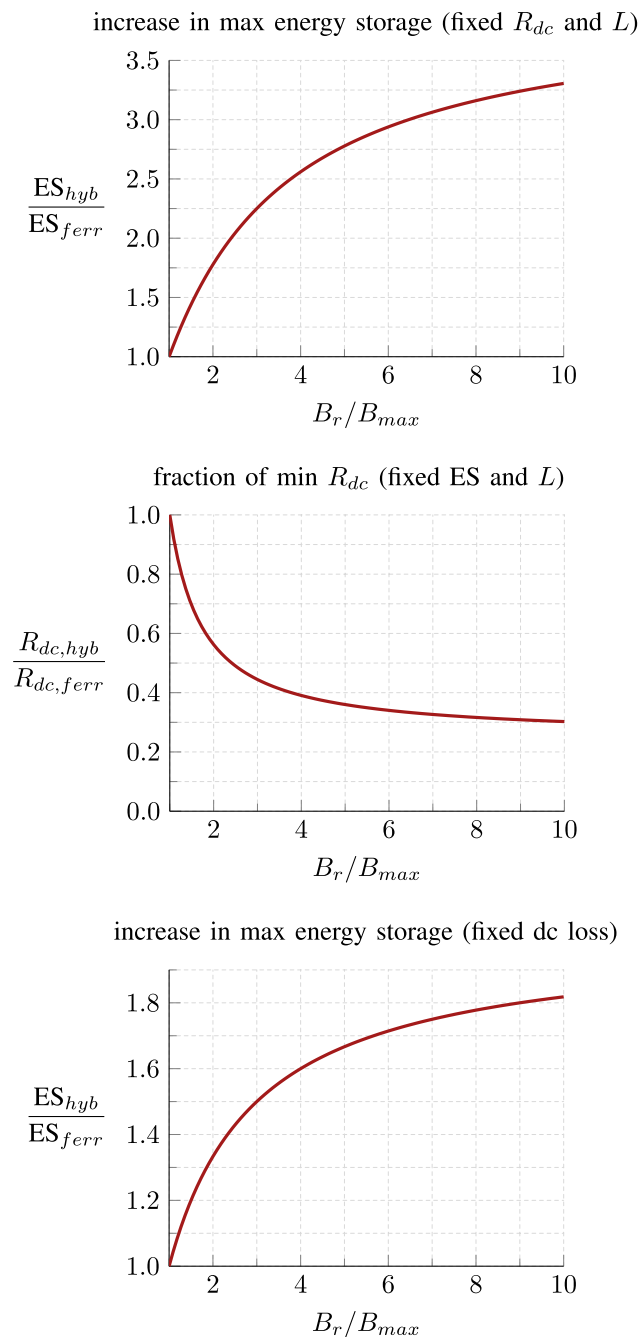


**FIGURE 5.** Performance comparisons between the PM hybrid core (ideal model) and ferrite core from Table 2. PM hybrid cores using PMs with larger  $B_r$ , compared to the ferrite's  $B_{max}$  can achieve better performance improvement, but substantial improvements are still possible at lower ratios of  $B_r/B_{max}$ .

the ratio between  $B_r$  and  $B_{max}$  increases. To understand how high this ratio needs to be to achieve substantial improvement, we plot these three metrics as a function of  $B_r/B_{max}$  in Fig. 5.

These plots show that the PM hybrid core can be advantageous at even relatively small ratios of  $B_r/B_{max}$ . For reference, the example comparisons in this subsection (summarized in Table 2) use materials with a ratio of  $B_r/B_{max} = 4$  and still achieve sizeable improvement for all three metrics.

For completeness, we also examine the upper bound in improvement for all three metrics in Table 2 as  $B_r/B_{max} \rightarrow \infty$ . In this limit, the PM hybrid core approaches the following improvements over a pure ferrite core:

- 1) 4x in energy storage for a fixed  $R_{dc}$  and  $L$
- 2) 0.25x in  $R_{dc}$  for a fixed energy storage and  $L$
- 3) 2x in energy storage for a fixed dc loss

So, to fully realize the PM hybrid core's potential for improvement, larger ratios of  $B_r/B_{max}$  are desirable. Larger ratios are achievable in cases where ferrites have particularly low saturation flux density ( $B_{sat} < 0.3$  T), which is common in materials designed for several MHz and above. Development of PM materials with greater  $B_r$  can also increase the PM hybrid core's advantages.

#### D. CORE LOSS IN THE PM HYBRID CORE

While strategically adding a PM to a ferrite can yield large flux carrying capabilities, the ferrite now has less area to carry ac flux, which increases core loss. However, for dc-dominated applications with small ac ripple, core loss in an inductor is much smaller than the copper loss. So, an increase in core loss will only have a small impact on the total loss and thus can be ignored.

To support this claim, we examine an example dc-dominated inductor design with small ac ripple current and compare the losses between a PM hybrid core and a pure ferrite core design. In this example, the inductor design specs are:  $L = 2 \mu\text{H}$ ,  $I_{dc} = 4.0$  A, peak ripple ratio  $I_{ac}/I_{dc} = 10\%$ , and frequency = 1 MHz. For this comparison, both cores use the same geometry: an E5.3/2.7/2 E-core geometry with a window fill factor of 50%. They also use the same ferrite material, 3F46 ( $B_{sat} = 0.43$  T at  $100^\circ\text{C}$ ).

For the pure ferrite design, we set the maximum core  $B$  field at  $B_{max} = 0.75B_{sat}$  to remain in the linear region of the BH curve. Using Dowell's equation to calculate copper loss and the Steinmetz equation to calculate core loss, we obtain a total of 140 mW of loss, with 139 mW of copper loss and 1.3 mW of core loss. The loss is thus extremely dominated by copper loss, with core loss only comprising 0.93% of the total loss.

Now, we examine how the copper and core losses change from this pure ferrite design to a PM hybrid core design. For simplicity, we fix dc resistance  $R_{dc}$  between the two cores and design the PM hybrid core to achieve its maximum energy storage for the same  $B_{max}$  in the ferrite part of the core (the first case in Table 2). As shown in Section II-C, in this case, we expect the PM hybrid core to achieve a factor of 2.56x more energy storage than the ferrite core.

Since  $R_{dc}$  is fixed,  $R_{ac}$  is also fixed, so the two cores have the same copper loss. To compare core loss in each core, we first calculate their peak ac  $B$  field using  $B_{ac} = LI_{ac}/(NA_{core})$ , where  $N$  is the number of turns and  $A_{core}$  is the ferrite core area in each core.  $L$  and  $I_{ac}$  are fixed by the design specifications and thus are the same in both cores. Because  $R_{dc}$  is fixed between the two cores,  $N$  is also the same. The two cores, though, have different ferrite core areas. While the pure ferrite design has a ferrite area equal to the total effective core area

$A_e$ , the PM hybrid core design has a ferrite area that is only a fraction of the total core  $A_e F_f$ . The PM hybrid core design thus has higher  $B_{ac}$  in its ferrite part than the pure ferrite core by a factor of  $B_{ac,hyb}/B_{ac,ferr} = 1/F_f$ .

However, core loss doesn't only depend on  $B_{ac}$ ; it also depends on the total ferrite core volume. Since the PM hybrid core has less ferrite volume ( $V_{core,hyb}/V_{core,ferr} = F_f$ ), the impact of increased  $B$  fields on core loss is somewhat tempered. To see the full impact of using less ferrite area on the PM hybrid design's core loss, we calculate core loss using the single-frequency form of the Steinmetz equation:  $P_{core} = V_{core} k B_{ac}^\beta$ , where  $V_{core}$  is the effective ferrite core volume and  $k$  and  $\beta$  are Steinmetz material parameters. The PM hybrid core thus has greater core loss compared to the pure ferrite core by a factor of

$$\begin{aligned} \frac{P_{core,hyb}}{P_{core,ferr}} &= \frac{V_{core,hyb} k B_{ac,hyb}^\beta}{V_{core,ferr} k B_{ac,ferr}^\beta} \\ &= \frac{V_{core,hyb}}{V_{core,ferr}} \left( \frac{B_{ac,hyb}}{B_{ac,ferr}} \right)^\beta \\ &= F_f \left( \frac{1}{F_f} \right)^\beta = F_f^{1-\beta} \end{aligned} \quad (10)$$

For our example ferrite material 3F46, we have  $\beta = 2.43$  at 1 MHz and 100 °C. To calculate  $F_f$ , we use the ideal PM hybrid core model (Section II-A, Table 1), which gives an optimal  $F_f = 0.80$  for a small-ripple design. Therefore, using (10), the PM hybrid core should have 38% more core loss than the ferrite core.

This increase may seem large, but again, in this example, core loss in the pure ferrite design is only 0.93% of the total loss. So moving to a PM hybrid core would only increase the total loss by 0.35%, a negligible increase and small price to pay for an energy storage increase of 2.56x (per Section II-C, Table 2). This example thus shows that the PM hybrid core can be greatly advantageous in dc-dominated, small-ripple applications, even at high frequencies.

For applications with larger ripple ratios, the PM hybrid design's increase in core loss will have a larger impact on the total loss. Still, the PM hybrid core may be advantageous in certain cases. This analysis, however, is beyond the scope of this article.

### III. PM HYBRID CORE IMPLEMENTATIONS

The example PM hybrid core implementation in Fig. 2 is just one of many potential implementations; many different core geometries and PM arrangements are possible. For more examples, we look at possible PM arrangements in a double u-core geometry in which the core is split into two symmetric u-shaped halves that are separated by two gaps (Fig. 6). Here, we look at two types of PM arrangements: 1) parallel PM arrangements and 2) non-parallel PM arrangements. PM implementations that use some combination of parallel and non-parallel placements are also possible.

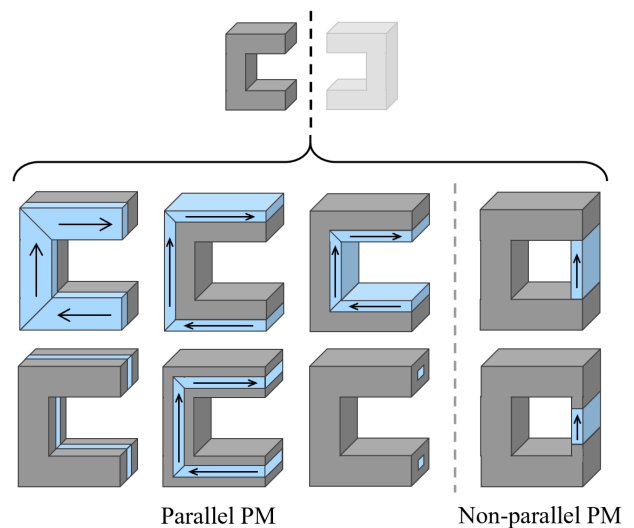


**FIGURE 6.** Example parallel and non-parallel arrangements of the PM hybrid core using a double u-core geometry. For simplicity, only one half of the double u-core is drawn. The PM sections in the core are drawn in light blue and the ferrite sections are drawn in grey.

For parallel PM arrangements, the PM is placed physically in parallel with the ferrite, as in the simple example in Fig. 2. In this case, the PM hybrid core can be treated as a single bulk material of PM and ferrite, as in the developed first-order models of Section II. In parallel PM arrangements, the PM can be placed alongside a single ferrite shape for simple construction, such as in the first row of Fig. 6. The PM can also be sandwiched or enclosed in the ferrite, such as in the last row of Fig. 6. Sandwiching or enclosing the PM encourages more of its flux to return through the ferrite instead of fringing outward and returning through the air. These arrangements also help the PM return flux better distribute in the ferrite.

For non-parallel PM arrangements, the PM is not *physically* placed in parallel with the ferrite, but it is still *magnetically* in parallel for its flux to oppose the dc winding flux in the ferrite. For example, in Fig. 6, the PM is placed perpendicular to the gap-side faces of the ferrite. In this case, the PM no longer needs to travel the same length as the ferrite, potentially saving volume. Modified models for these arrangements are beyond the scope of this article.

In all PM arrangements, the junction where the PM flux returns into the ferrite can be critical for the PM hybrid core's saturation capability [22]. For example, in cases where the end of the PM interfaces directly with the ferrite, such as in non-parallel PM arrangements, the PM flux at this interface may flow perpendicular to the dc winding flux. Instead of offsetting the dc winding flux, this perpendicular PM flux contributes to the ferrite's saturation near this junction. To compensate for this issue, we can increase the cross-sectional ferrite area for the dc winding flux near this interface, as in the bottom right example in Fig. 6. Alternatively, material can be added to guide the PM flux to return parallel to the dc winding flux in the desired ferrite areas. An example such PM hybrid design that uses steel flux guides is presented in the next section.

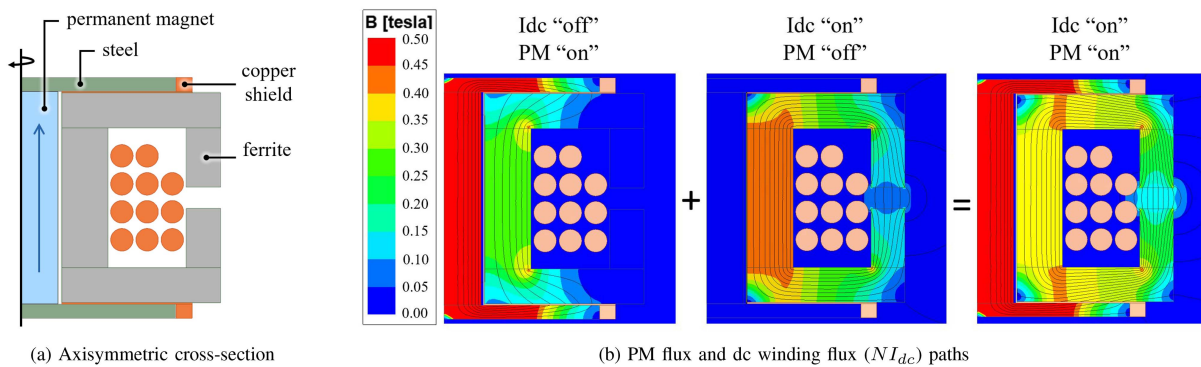


**FIGURE 7.** An example PM hybrid core inductor using a pot core geometry, with the PM magnetized in the z-direction. The PM offsets the flux in the center post (see  $I_{dc}$  “off”, PM “on”) but does not see flux induced by the winding (see  $I_{dc}$  “on”, PM “off”).

**TABLE 3.** Specifications for the Prototype Inductors

	PM Hybrid	Pure Ferrite (fixed $I_{dc,max}$ )	Pure Ferrite (fixed $R_{dc}$ )
L (at 1 MHz)	35.1 $\mu$ H	35.1 $\mu$ H	35.1 $\mu$ H
Core Material(s)	PM: N40SH ( $B_r = 1.285$ T, 6 pcs, $\varnothing 4$ mm x 2 mm ht each) Ferrite: 3F46 ( $B_{sat} = 0.43$ T at 100 °C, P22/13, modified) Steel: Hiperco-50 (5 laminations, $\varnothing 16.8$ mm, 0.76 mm ht total)	3F46 (P22/13/I)	3F46 (P22/13/I)
Shield	Inner Ring: ID 4.4 mm, OD 18.5 mm, 65 $\mu$ m ht Outer Ring: ID 16.8 mm, OD 18.5 mm, 0.76 mm ht	—	—
Gap Length	0.74 mm (outer gap)	2.3 mm (outer gap)	0.76 mm (outer gap)
Winding	11 turns (16 AWG)	15 turns (18 AWG)	11 turns (16 AWG)

#### IV. A NON-OPTIMIZED PROOF-OF-CONCEPT DESIGN

For proof of concept, we designed and built an example PM hybrid core inductor using readily-available ferrite cores and PMs (Fig. 7). Specifications for this design are listed in Table 3 for intended operation at 1 MHz. In addition to ferrite and a PM, this example design uses steel and copper shields to help direct flux throughout the core structure. The design has the same total volume as a size P22/13 pot core; the center post and outer shell heights of the ferrite pot core were ground down to compensate for the added steel volume. Since this prototype uses off-the-shelf parts, it was not designed to achieve the optimized ideal characteristics in Section II-A; an optimized design may be expected to perform better than this initial prototype.

##### A. GENERAL DESIGN

For its base geometry, this example PM hybrid core inductor uses a size P22/13 ferrite pot core with a center hole in which a PM can easily be incorporated. In this geometry, though, the core area is not constant throughout, introducing additional design considerations to the strategies from Section II. To maximize saturation performance in this case, we want to prioritize offsetting the winding flux in the regions of the pot core with the smallest cross-sectional areas, as they are the most limiting for saturation. In the P22/13 pot core, the smallest area is in the center post with  $A_{post} = 54.2$  mm<sup>2</sup>. A close second is the radial area of the end caps (the top and

bottom sections) at the center post’s outer diameter, which has  $A_{cap} = 56.7$  mm<sup>2</sup>. (At larger diameters, the end caps’ area increases and becomes less limiting for saturation.) In contrast, the outer shell of the pot core has the largest area at  $A_{shell} = 114.4$  mm<sup>2</sup>, about 2x greater than the center post area. So, to improve the ferrite pot core’s saturation behavior, we focus on utilizing the PM to offset the dc winding flux in the center post and end cap regions near it.

To do this, a steel disc<sup>2</sup> is added on either end of the pot core, flush with the PM in the center hole (Fig. 7(a)). The steel, with a higher permeability than ferrite, guides the PM flux radially outward along the end cap. The steel is designed to be just thick enough to support the PM flux without saturating. Thicker steel would use extraneous volume in the inductor that could be better utilized to increase its saturation capability or reduce its losses. For selecting the radius of the steel discs, see Section IV-C.

To encourage the PM flux in the steel to return through the ferrite end caps and center post, the inductor’s gap is placed in the outer shell. Meanwhile, the winding flux flows through the ferrite pot core and across the outer gap. Negligible winding flux flows through the PM, as the permeance of the PM is

<sup>2</sup>The prototype uses a laminated steel disc made of Hiperco-50 due to its availability. Hiperco-50 has a nominal permeability  $\mu_r = 12000$  and nominal  $B_{sat} = 2.4$  T. See design details in Table 3.

much smaller than that of the ferrite center post. Fig. 7(b) plots dc flux lines for this geometry.

### B. PM DESIGN

To maximize the flux carrying capability in this PM hybrid design, we ideally want a PM that can provide the same magnitude of flux as the maximum dc winding flux in the center post and end cap regions near it. With such a PM to reverse bias flux, these regions would have double the flux density range and achieve the same maximum flux carrying capability as the outer shell, which has twice the cross-sectional area but only a unidirectional flux density range. The center post, end cap regions near it, and the outer shell would then saturate at roughly the same time, taking greater advantage of the material's saturation capabilities.

To find the maximum flux carrying capability of the ferrite, for this design, we set  $B_{\max} = 0.75B_{\text{sat}}$  to remain in the linear region of the ferrite's BH curve. The maximum dc winding flux in the center post and end cap regions is thus  $\phi_{\max, \text{ferr}} = B_{\max}A_{\text{post}} = 0.32 \text{ T}(54.2 \text{ mm}^2) = 17.5 \mu\text{Wb}$ .

Ideally, our PM should match this flux. There's some flexibility in choosing which PM to use, as the PM flux can be tuned through its material property  $B_r$  or cross-sectional area  $A_{\text{PM}}$  via  $\phi_{\text{PM}} = B_r A_{\text{PM}}$ . But the maximum  $B_r$  is limited by available materials, and for this example design, the maximum PM area is limited by the center hole area. Considering these constraints, we chose a readily-available PM (Table 3) that provides the greatest flux within the center hole area without reverse saturating the core at zero current. This PM provides a flux of  $16.1 \mu\text{Wb}$ , which is 92% of the maximum dc winding flux in the center post and end cap regions near it.

### C. SHIELD DESIGN

While guiding dc flux is important for higher effective saturation in this example design, guiding ac flux is also necessary for low loss. In particular, ac flux should be avoided in the PM and steel, which can both incur large ac losses. In the center post region, avoiding ac flux in the PM is not a problem since ac flux prefers the ferrite over the PM, which generally has much smaller permeability at around  $\mu_0$ .<sup>3</sup> However, for the end cap regions, some ac flux could exit the ferrite into the higher-permeability steel, incurring eddy current loss in the steel. To prevent this, copper shields are added between the ferrite and steel to reject ac flux but still allow dc flux to pass.

The shields' geometry is designed to reduce loss using minimal volume. For construction, each shield can be broken into two parts: an inner shield ring that sits between the ferrite and steel, and an outer shield ring that fits around the steel disc. The outer ring provides additional conduction area to reduce eddy current losses in the shields. The inductor is intended for operation at 1 MHz (Table 3), so the inner shield ring thickness is designed to be around one skin depth at  $65 \mu\text{m}$ .

<sup>3</sup>For PM hybrid cores that use soft magnetic materials with much lower permeability (e.g. powder core materials), a copper shield can be added between the soft magnetic material and PM.

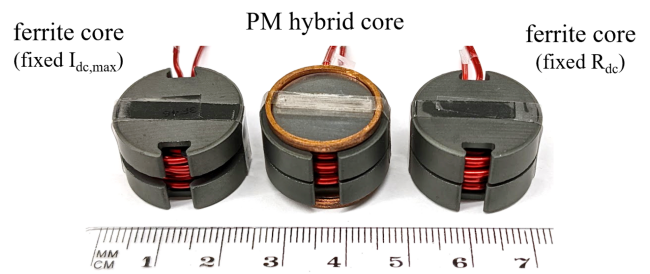


FIGURE 8. Prototypes of the pure ferrite and PM hybrid core inductors.

The inner shield ring's inner diameter is set by the pot core's center hole diameter.

Designing the outer diameter (OD) of the shield, though, is more complex and ties into the design of the steel end cap's diameter. As the shield's OD increases, the shield rejects more ac flux from the ferrite but at the expense of greater eddy currents, and thus losses, in the shield. Decreasing the shield's OD, though, restricts the diameter of the steel disc, limiting its ability to guide dc flux radially outward along the end caps. In this case, the PM flux offsets dc winding flux in a smaller area of the ferrite core, reducing the PM hybrid core's saturation capability. Therefore, an optimal shield OD (and steel diameter) exists that balances saturation capability in the ferrite end caps with shield losses. For this example design, we found this optimum manually using finite element analysis (FEA) simulation.

### D. SIMULATION AND EXPERIMENTAL RESULTS

The example PM hybrid core inductor design was simulated using 2D cylindrical FEA in ANSYS Maxwell 21.2, with ferrite core data at  $100^\circ\text{C}$  and copper resistivity at  $75^\circ\text{C}$ . The design's saturation behavior was characterized in simulation and experiment via its inductance behavior across dc current.<sup>4</sup> To verify that the PM offset the dc winding flux as designed, the example design was also simulated and measured without the PM.

In both simulation and experiment, the PM hybrid prototype (Fig. 8) achieved much greater saturation current with the PM than without it, indicating that the PM was indeed offsetting the dc winding flux (Fig. 9). For a 30% allowable drop in inductance, the PM hybrid prototype achieved a dc current of 11.1 A in simulation with a dc resistance of  $R_{\text{dc}} = 8.5 \text{ m}\Omega$  and 10.0 A in experiment with  $R_{\text{dc}} = 7 \text{ m}\Omega$ . For the same inductance drop without the PM, the inductor experimentally achieved 6.9 A; thus, the PM improved the inductor's maximum dc current by 45%.

The discrepancy in the PM hybrid inductor's saturation behavior between simulation and experiment can partially be attributed to the 2D FEA simulations not fully capturing 3D effects in the pot core geometry, particularly near the two vertical slots for winding terminations that cut into the end caps. This geometric asymmetry caused

<sup>4</sup>For details on the experimental setup, see Appendix A.

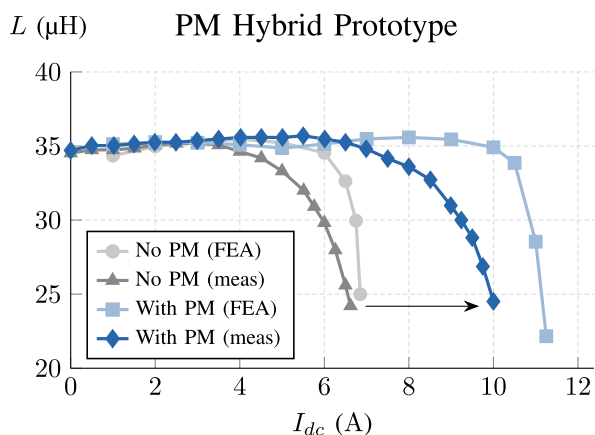


**FIGURE 9.** Simulated and measured saturation behavior of the PM hybrid inductor with and without the PM. Adding the PM to this inductor design greatly improved its saturation behavior, indicating that the PM flux was offsetting the dc winding flux as designed.

the ferrite core (without the PM) to saturate unevenly in these regions and the center post, resulting in poorer experimental saturation behavior than in 2D simulations, as shown in Fig. 9. Therefore, the reduced maximum dc current in the PM hybrid prototype was partially due to discrepancies separate from the PM hybrid core design.

A source of discrepancy related to the PM hybrid design is the physical implementation of the off-the-shelf PM. Instead of a single uncoated PM rod, the PM was a stack of six shorter PMs, each with nickel coating. This coating introduced gaps between the PM and steel and also provided a magnetic shunt path for the PM flux, thus reducing the amount of PM flux opposing the dc winding flux in the ferrite. With the nickel magnetic shunt path, any additional small gaps between the PM and steel, even on the order of tens of microns, could have also further reduced the prototype’s saturation performance.

As an example, we simulated a version of the PM hybrid design that aligns more closely with the prototype PM and compared it with the original simulated results (Fig. 10). The PM was simulated in six sections, each with a 25 μm-thick nickel coating, per the datasheet. Gaps of 65 μm each were also added between the ends of the PM and the steel. Fig. 10 shows that these modifications to the PM can substantially reduce the PM hybrid prototype’s performance and thus partially explain the experimental discrepancy.

### E. COMPARISON TO FERRITE CORES

To highlight the PM hybrid core’s benefits, the example design was compared to two pure ferrite pot core designs having the same volume and inductance (see specs in Table 3). The ferrite designs used a conventional P22/13/I core without a center hole and had the same total component volume as the PM hybrid design (Fig. 8). Two ferrite inductor comparisons were used to demonstrate two different ways of leveraging the PM hybrid core’s greater flux carrying capability for improved performance. Results for both ferrite prototypes are shown in Fig. 11 and Table 4. Unlike the PM hybrid prototype,

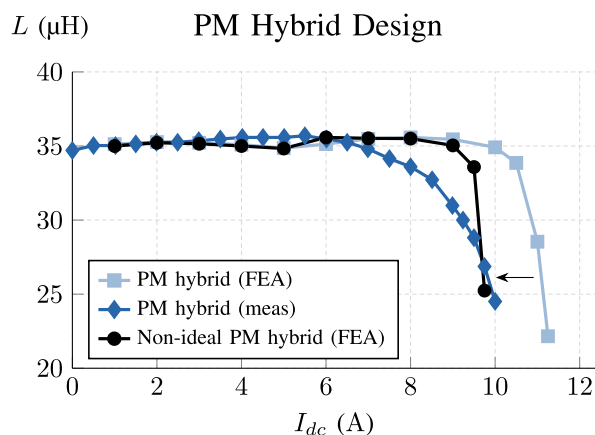


**FIGURE 10.** Simulated saturation behavior of the PM hybrid design with construction non-idealities compared to the original results of the PM hybrid prototype. The non-ideal PM hybrid design simulates the PM in six sections, each with a 25 μm-thick nickel coating. 65 μm gaps are also added between the PM and steel on either end. These non-idealities reduce the PM hybrid design’s simulated saturation performance, partially explaining the poorer experimental performance.

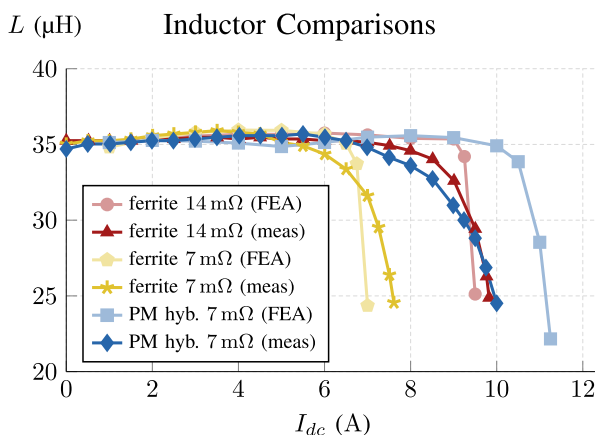


**FIGURE 11.** Simulated and measured saturation behavior of the PM hybrid and pure ferrite inductors. In experiment, the PM hybrid prototype achieved half the dc resistance of a ferrite prototype with similar saturation behavior (ferrite 14 mΩ). For a 30% allowable drop in inductance, the PM hybrid prototype achieved 30% more dc current, and thus 70% more energy storage, than a ferrite prototype with the same dc resistance (ferrite 7 mΩ).

the ferrite prototypes did not have much poorer experimental saturation behavior compared to simulations due to their geometries having larger center post areas, making them more resilient to the 3D effects of uneven saturation in the end caps.

One ferrite comparison inductor was designed to have similar saturation behavior as the PM hybrid prototype, and their dc resistances were compared. For a 30% allowable drop in inductance, the ferrite prototype achieved 9.5 A of dc current in simulation with  $R_{dc} = 12.9 \text{ m}\Omega$  and 9.7 A in experiment with  $R_{dc} = 14 \text{ m}\Omega$ . For the same inductance drop, the PM hybrid prototype experimentally achieved the same maximum dc current as the ferrite prototype, and thus the same energy storage, at only half the dc resistance.

**TABLE 4. Experimental Results for the Prototype Inductors. Maximum Values are Calculated for a 30% Allowable Drop in  $L$**

	Pure Ferrite (fixed $I_{dc,max}$ )	PM Hybrid	Pure Ferrite (fixed $R_{dc}$ )
$R_{dc}$	14 m $\Omega$	$\xrightarrow{0.5x}$ 7 m $\Omega$	7 m $\Omega$
max $I_{dc}$	9.7 A	10.0 A	$\xleftarrow{1.3x}$ 7.6 A
max energy storage	1.2 mJ	1.2 mJ	$\xleftarrow{1.7x}$ 0.7 mJ

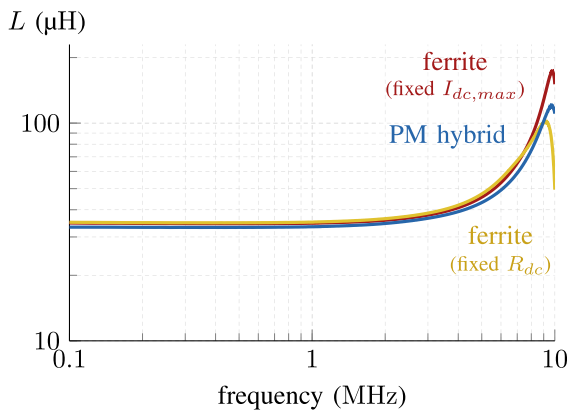


**FIGURE 12. Measured inductance across frequency of the PM hybrid and pure ferrite inductors. All prototypes have similar behavior.**

The other ferrite comparison inductor was designed at the same dc resistance as the PM hybrid prototype at  $R_{dc} = 7\text{ m}\Omega$ , and their maximum dc currents (and energy storage) were compared. For a 30% allowable drop in inductance, the ferrite prototype achieved 7.0 A of dc current in simulation with  $R_{dc} = 8.6\text{ m}\Omega$  and 7.6 A in experiment with  $R_{dc} = 7\text{ m}\Omega$ . For the same inductance drop, the PM hybrid inductor experimentally achieved 30% greater maximum dc current, and thus 70% greater energy storage, than the ferrite prototype. So, even with a non-optimal proof-of-concept design, the PM hybrid core outperformed ferrite designs at the same volume, demonstrating its potential performance advantages.

The inductance behaviors of the ferrite and PM hybrid core prototypes were also characterized across frequency at zero dc current using an impedance analyzer (Agilent 4395 A) (Fig. 12). All prototypes had similar behavior, suggesting that the PM hybrid core implementation does not introduce additional effects on inductance.

## V. CONCLUSION

For power applications in which an inductor will be saturation-limited, a PM hybrid core can improve energy storage density or loss by providing greater effective saturation flux density. To achieve this, some fraction of the core material is replaced by a PM to offset dc winding flux in the rest of the core, thus allowing the core material to use a greater range of the BH curve. A proof-of-concept PM hybrid core inductor was designed and built using off-the-shelf parts. For a fixed

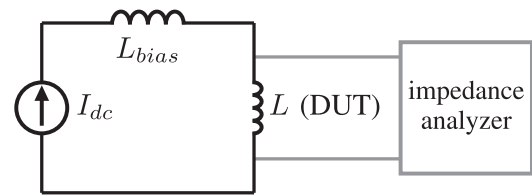


**FIGURE 13. Schematic of the saturation behavior measurement setup.**

**TABLE 5. Specifications for the Bias Inductor Used in the Saturation Behavior Measurement Setup**

L (at 1 MHz)	490 $\mu\text{H}$
Core Material	N87
Core Geometry	PM 87/70
Gap Length	2.5 mm (center & outer gaps)
Winding	36 turns (AWG 10)

energy storage, this non-optimized prototype experimentally achieved half the dc resistance of a pure ferrite core inductor at the same volume and core area. For a fixed dc resistance, the prototype also achieved 70% more energy storage than a comparable ferrite inductor. Optimized PM hybrid core designs may potentially achieve even greater performance.

## APPENDIX A SATURATION BEHAVIOR MEASUREMENT SETUP

To measure the saturation behavior of the prototype inductors, we biased them at different levels of dc current with a dc power supply (HP 6012 A) and then measured their inductances on an impedance analyzer (Agilent 4395 A). A schematic of the experimental setup is shown in Fig. 13.

For accurate inductance measurements with the impedance analyzer, the dc supply must present an impedance much larger than the device under test (DUT). Therefore, a bias inductor with a very large inductance, much greater than the prototypes' inductances, was added in series with the supply. To ensure that the bias inductor does not affect the DUT measurements, it was designed to saturate at a dc current  $> 15\text{ A}$ , much larger than the expected saturation currents of the prototypes. The bias inductor was also designed to have a relatively small temperature rise ( $< 40^\circ\text{C}$ ) at full load to ensure stable behavior across current. For bias inductor specs, see Table 5.

We experimentally verified that the bias inductor does not saturate below 15 A. To do this, we built a second identical bias inductor to serve as the DUT. We then measured the inductances of the two bias inductors in parallel across dc current and found that they were stable up to 20 A.

## REFERENCES

- [1] R. S. Yang, A. B. Nadler, C. R. Sullivan, and D. J. Perreault, "Permanent magnet hybrid core inductors for high saturation capability," in *Proc. IEEE 23rd Workshop Control Model. Power Electron.*, 2022, pp. 1–8.
- [2] J. Muhlethaler, J. Biela, J. W. Kolar, and A. Ecklebe, "Core losses under the DC bias condition based on Steinmetz parameters," *IEEE Trans. Power Electron.*, vol. 27, no. 2, pp. 953–963, Feb. 2012.

- [3] E. Stenglein and T. Dürbaum, "Core loss model for arbitrary excitations with DC bias covering a wide frequency range," *IEEE Trans. Magn.*, vol. 57, no. 6, Jun. 2021, Art. no. 6302110.
- [4] A. J. Hanson, J. A. Belk, S. Lim, C. R. Sullivan, and D. J. Perreault, "Measurements and performance factor comparisons of magnetic materials at high frequency," *IEEE Trans. Power Electron.*, vol. 31, no. 11, pp. 7909–7925, Nov. 2016.
- [5] Y. Han, G. Cheung, A. Li, C. Sullivan, and D. Perreault, "Evaluation of magnetic materials for very high frequency applications," *IEEE Trans. Power Electron.*, vol. 27, no. 1, pp. 425–435, Jan. 2012.
- [6] M. S. Rylko, B. J. Lyons, J. G. Hayes, and M. G. Egan, "Revised magnetics performance factors and experimental comparison of high-flux materials for high-current DC–DC inductors," *IEEE Trans. Power Electron.*, vol. 26, no. 8, pp. 2112–2126, Aug. 2011.
- [7] M. Kacki, M. S. Rylko, J. G. Hayes, and C. R. Sullivan, "Magnetic material selection for EMI filters," in *Proc. IEEE Energy Convers. Congr. Expo.*, 2017, pp. 2350–2356.
- [8] T. Fujiwara and H. Matsumoto, "A new downsized large current choke coil with magnet bias method," in *Proc. 25th Int. Telecommun. Energy Conf.*, 2003, pp. 416–420.
- [9] R. Wrobel, N. McNeill, and P. H. Mellor, "Design of a high-temperature pre-biased line choke for power electronics applications," in *Proc. IEEE Power Electron. Specialists Conf.*, 2008, pp. 3171–3177.
- [10] G. M. Shane and S. D. Sudhoff, "Design and optimization of permanent magnet inductors," in *Proc. IEEE Appl. Power Electron. Conf. Expo.*, 2012, pp. 1770–1777.
- [11] J. Friebe, "Permanentmagnetische vormagnetisierung von speicherdrosseln in stromrichtern," Ph.D. dissertation, Dept. Electr. Eng./Comput. Sci., Univ. Kassel, Kassel, Germany, 2014.
- [12] Z. Dang and J. A. Abu Qahouq, "Permanent magnet toroid power inductor with increased saturation current," in *Proc. IEEE Appl. Power Electron. Conf. Expo.*, 2013, pp. 2624–2628.
- [13] Z. Dang and J. A. Abu Qahouq, "Evaluation of high-current toroid power inductor with NdFeB magnet for DC–DC power converters," *IEEE Trans. Ind. Electron.*, vol. 62, no. 11, pp. 6868–6876, Nov. 2015.
- [14] Z. Dang and J. A. Abu Qahouq, "Permanent-magnet coupled power inductor for multiphase DC–DC power converters," *IEEE Trans. Ind. Electron.*, vol. 64, no. 3, pp. 1971–1981, Mar. 2017.
- [15] Z. Xia, J. A. Abu Qahouq, and S. Kotru, "Evaluation of permanent magnet distribution schemes for toroid power inductor with increased saturation current using 3D physical models," in *Proc. IEEE Appl. Power Electron. Conf. Expo.*, 2019, pp. 2894–2899.
- [16] S. Lin, J. Friebe, S. Langfermann, and M. Owzareck, "Premagnetization of high-power low-frequency dc-inductors in power electronic applications," in *Proc. Power Convers. Intell. Motion Europe*, 2019, pp. 1–7.
- [17] J. Friebe, S. Lin, L. Fauth, and T. Brinker, "Premagnetized inductors in single phase DC-AC and AC-DC converters," in *Proc. IEEE 15th Braz. Power Electron. Conf. 5th IEEE Southern Power Electron. Conf.*, 2019, pp. 1–6.
- [18] J. Friebe and P. Zacharias, "Review of magnetic material degradation characteristics for the design of premagnetized inductors," *IEEE Trans. Magn.*, vol. 50, no. 3, Mar. 2014, Art. no. 4003809.
- [19] N. Yogal, C. Lehrmann, and M. Henke, "Measurement of eddy current loss in permanent magnets with high-frequency effects of electrical machines for hazardous locations," in *Proc. 22nd Int. Conf. Elect. Mach. Syst.*, 2019, pp. 1–5.
- [20] A. Revilla Aguilar and S. Munk-Nielsen, "Half size reduction of DC output filter inductors with the saturation-gap magnetic bias topology," *IEEE Trans. Emerg. Sel. Topics Power Electron.*, vol. 4, no. 2, pp. 382–392, Jun. 2016.
- [21] W. G. Hurley and W. H. Wölfle, *Transformers and Inductors for Power Electronics: Theory, Design and Applications*, 1st ed. Hoboken, NJ, USA: Wiley, 2013.
- [22] B. Houska, D. Yan, J. Benzaquen, and D. Divan, "Partial saturation in permanent magnet inductors," in *Proc. IEEE Energy Convers. Congr. Expo.*, 2022, pp. 1–7.